Analysis of the Absorption and Magnetic Circular Dichroism Spectra of Iron(II) Phthalocyanine

Edward A. Ough and Martin J. Stillman*

Department of Chemistry, The University of Western Ontario, London, Ontario, N6A 5B7 Canada

Received June 9, 1993®

Assignments for the absorption and magnetic circular dichroism (MCD) spectra recorded between room temperature and 50 K are reported for a range of iron(II) phthalocyanine complexes, with axial ligands of imidazole, *N*-methylimidazole, pyridine, methylpyridine, piperidine, ammonia, cyanide, and carbon monoxide. The L_2Fe^{II}-Pc(-2) complexes can be arranged into three distinct groups on the basis of the spectral features according to the σ donor and π acceptor strengths of the axial ligands: (1) strong σ donors–weak π acceptors [L = im, meim, py, mepy, pip, and NH_3]; (2) weak σ donors–strong π acceptors [L = CO]; and (3) strong σ donors–weak π donors [$L = CN^-$]. The complexes $(NH_3)_2Fe^{II}Pc(-2)$, $(NH_3)(CO)Fe^{II}Pc(-2)$, and $Na_2[(CN)_2Fe^{II}Pc(-2)]$ are representative of these three groups. Parameters reported from band deconvolution calculations carried out on pairs of absorption and MCD spectra provide quantitative support for the characterization of these complexes as members of three groups. Results from the deconvolution calculations are used to locate two degenerate ligand to metal charge transfer (LMCT) transitions between 300 and 450 nm in addition to a series of π–π^* transitions based on the phthalocyanine ring. Degenerate π–π^* ring states are assigned for the Q, B1, B2, N, and L transitions; in addition, two LMCT bands, representing the allowed $e_g(d\pi) \rightarrow 1b_{1u}(\pi^*)$ and $e_g(d\pi) \rightarrow 1b_{2u}(\pi^*)$ transitions, are characterized from the MCD spectral analysis. Degenerate states are identified from the MCD A terms: 662 (Q_{00}), 424 (MLCT1), 359 (MLCT2), 341 (B1), 316 (B2), 273 (N), and 253 nm (L) for $(NH_3)_2Fe(II)Pc(-2)$; 665 (Q_{00}), 453 (MLCT1), 396 (B1), 334 (MLCT2), 307 (B2), 279 (N), and 251 nm (L) for $Na_2[(CN)_2Fe(II)Pc(-2)]$; and 659 (Q_{00}), 369 (MLCT1), 352 (MLCT2), 327 (B1), 307 (B2), and 278 nm (L) for $(NH_3)(CO)Fe(II)Pc(-2)$.

Introduction

The chemistry of the metallophthalocyanine molecule has been extensively studied over the past 50 years.[1] The interest in these metallomacrocycles arises from their intense coloration and diverse redox chemistry associated with both the aromatic 18-π-electron system of the phthalocyanine ring and the central metal[1,2] Because of the enhanced chemical and thermal stability compared with the parent porphyrins, there is also considerable interest in the metallophthalocyanines as industrial dyes, as potential photosensitizers in the conversion of solar energy to chemical or electrochemical energy,[3,4] for use in the photodynamic treatment (PDT) of cancer,[5] as one-dimensional molecular metals,[6–10] and as sensors for the quantitative detection of atmospheric pollutants.[11] In spite of the extent of these practical chemical applications, full exploitation of the chemical properties of this class of molecules is hindered by our limited knowledge of the electronic structures of the ground and excited states. Analysis of high-quality electronic absorption and magnetic circular dichroism (MCD) spectra provides direct information about energies and degeneracies of states in the 1.0–6.0-eV region.[2a]

Spectral studies of the "simple" metallophthalocyanines, represented by magnesium phthalocyanine (MgPc(-2))[2a,12] and zinc phthalocyanine (ZnPc(-2)),[2a,13–15] are invaluable in advancing our understanding of the electronic properties of the phthalocyanine ring itself. In these highly symmetric complexes the Mg(II) and Zn(II) are chromophorically and electrochemically silent, with the spectral band intensity arising entirely from phthalocyanine ring-based electronic transitions.[2a] Band analysis of the absorption and magnetic circular dichroism (MCD) spectra of MgPc(-2) and ZnPc(-2) have defined the energies and polarization properties of state to state transitions of the phthalocyanine ring. However, when the central metal is either or both spectrally and electrochemically active, quite different spectra are observed, and these spectra directly reflect new chemistry that can take place at either the ring or the central metal (some of these spectral data are summarized in ref 2a). In particular, the lack of chemistry at the metal site makes MgPc-(-2) and ZnPc(-2) poor models of complex systems in which the metal–ring interaction results in the significant chemistry observed

* Address correspondence to this author (Internet: STILLMAN@UWO.CA).

® Abstract published in *Advance ACS Abstracts*, January 1, 1994.

(1) (a) *Phthalocyanines: Properties and Applications*; Leznoff, C. C., Lever, A. B. P., Eds., VCH Publications: New York, 1989; Vol. 1. (b) *Phthalocyanines: Properties and Applications*; Leznoff, C. C., Lever, A. B. P., Eds., VCH Publications: New York, 1992; Vol. 2. (c) *Phthalocyanines: Properties and Applications*; Leznoff, C. C., Lever, A. B. P., Eds., VCH Publications: New York, 1993; Vol. 3.

(2) (a) Stillman, M. J.; Nyokong, T. In *Phthalocyanines: Properties and Applications*; Leznoff, C. C., Lever, A. B. P., Eds., VCH Publications: New York, 1989; Vol. 1, Chapter 3, pp 133–289. (b) Lever, A. B. P.; Milaeva, E. R.; Speier, G. In *Phthalocyanines: Principles and Applications*; Leznoff, C. C., Lever, A. B. P., Eds., VCH Publications: New York, 1993; Vol. 3, Chapter 1, pp 3–69.

(3) Darwent, J. R.; Douglas, P.; Harriman, A.; Porter, G.; Richoux, M. C. *Coord. Chem. Rev.* **1982**, *44*, 83–125.

(4) Elliot, C. M.; Hershenhart, E. J. *J. Am. Chem. Soc.* **1982**, *104*, 7519–7526.

(5) Spikes, J. D. *Photochem. Photobiol.* **1986**, *43*, 691.

(6) Palmer, S. M.; Stanton, J. L.; Martinsen, J.; Ogawa, M. Y.; Heuer, W. B.; Van Wallendael, S. E.; Hoffman, B. M.; Ibers, J. A. *Mol. Cryst. Liq. Cryst.* **1985**, *125*, 1–11.

(7) Yamakado, H.; Yakushi, K.; Kosugi, N.; Kuroda, H.; Kawamoto, A.; Tanaka, J.; Sugano, T.; Kinoshita, M.; Hino, S. *Bull. Chem. Soc. Jpn.* **1989**, *62*, 2267–2272.

(8) Almeida, M.; Kanatzidis, M. G.; Tonge, L. M.; Marks, T. J.; Marcy, H. O.; McCarthy, W. J.; Kannewurf, C. R. *Solid State Commun.* **1987**, *63*, 457–461.

(9) Hoffman, B. M.; Ibers, J. A. *Acc. Chem. Res.* **1983**, *16*, 15–21.

(10) Marks, T. J. *Science* **1985**, *227*, 881–889.

(11) Temofonte, T. A.; Schoch, K. F. *J. Appl. Phys.* **1988**, *65(3)*, 1350–1355.

(12) Ough, E. A.; Nyokong, T.; Creber, K. A. M.; Stillman, M. J. *Inorg. Chem.* **1988**, *27*, 2725–2732.

(13) Nyokong, T.; Gasyna, Z.; Stillman, M. J. *Inorg. Chem.* **1987**, *26*, 1087–1095.

(14) Nyokong, T. N. Ph.D. Thesis, The University of Western Ontario, London, Ontario, Canada, 1986.

(15) (a) Nyokong, T.; Gasyna, Z.; Stillman, M. J. *Inorg. Chem.* **1987**, *26*, 548–553; (b) Nyokong, T.; Gasyna, Z.; Stillman, M. J. *Inorg. Chim. Acta* **1986**, *112*, 11–15.

0020-1669/94/1333-0573$04.50/0

for iron porphyrins.[1] In these complexes, electronic overlap between the central ferrous atom and ring can be observed from charge transfer (CT) transitions between iron and the porphyrin ligand and point to extensive coupling between the two electronic systems. These charge transfer transitions comprise a significant portion of the observed spectral envelope between 200 and 1000 nm.[2a,16,17] Because the Q and B1/B2 bands in the phthalocyanines are so well separated (at 670 and 360 nm, respectively) when compared with the analogus α and Soret (or γ) bands of the porphyrins, analysis of the spectral data of $Fe^{II}Pc(-2)$ can provide very accurate information on the number, energy, and position of both MLCT and LMCT bands: data that allow assessment of the extent of the coupling between the ring and the metal.

In this paper, absorption and MCD spectra for a variety of low-spin diamagnetic $L_2Fe^{II}Pc(-2)$ complexes are reported. The axial ligands (L) included in this study are: carbon monoxide (CO), imidazole (im), *N*-methylimidazole (meim), pyridine (py), 4-methylpyridine (mepy), ammonia (NH_3), piperidine (pip) and cyanide (CN^-). Spectral band deconvolution calculations are used to assign band center energies, bandwidths, and magnetic moments of the transitions that contribute to the spectral envelopes in the absorption and MCD spectra. Results from previous spectroscopic studies of $MgPc(-2)$[2a,12] and $ZnPc(-2)$[2a,13-15] are used to identify the "pure" ($\pi \rightarrow \pi^*$) phthalocyanine ring-based transitions and isolate the new CT bands. The energies of the CT bands are compared with those predicted on the basis of electrochemical redox potentials.[18]

Experimental Section

Materials and Methods. $Fe^{II}Pc(-2)$ (Kodak) was purified by repeated (three times) vacuum sublimation. The fragmentation pattern in the mass spectrum of the purified $Fe^{II}Pc(-2)$ was checked to ensure that there was no modification of the peripherally fused benzene rings. Imidazole (im; Fisher), sodium cyanide (NaCN; Fisher), pyridine (py; BDH), 4-methylpyridine (mepy; BDH), piperidine (pip; BDH), methylimidazole (meim; Aldrich), carbon monoxide (CO; Union Carbide), ammonia (NH_3; Union Carbide), 1,1-dichloromethane (DCM; BDH), *N*,*N*-dimethylformamide (DMF; BDH), and *N*,*N*-dimethylacetamide (DMA; BDH) were used without further purification. $L_2M^{II}Pc(-2)$ (L = im, meim, py, mepy, pip, CN^-; M = Mg, Fe) was prepared according to literature methods.[12-15,19] $(NH_3)_2Fe^{II}Pc(-2)$ was prepared by bubbling ammonia gas (NH_3) through a suspension of 1.0 mg of $Fe^{II}Pc(-2)$ in 25 mL of DCM for 30 min. The solution was filtered to remove solid $Fe^{II}Pc(-2)$. The absorption spectra closely resembled those previously published.[2a,26,27] $(NH_3)(CO)Fe^{II}Pc(-2)$ was prepared by bubbling carbon monoxide (CO) through a DCM solution of $(NH_3)_2Fe^{II}Pc(-2)$ for 1 h. Absorption spectra were measured every 5 min to follow the conversion from $(NH_3)_2Fe^{II}Pc(-2)$ to $(NH_3)(CO)Fe^{II}Pc(-2)$, until no further changes occurred.

Spectroscopic Methods. All solution spectra were recorded from nitrogen-saturated DCM solutions. Spectra were measured in 1-cm path length square UV cells or 1-cm path length cylindrical MCD cells. Low-temperature absorption and MCD spectra were measured on glassy solutions prepared in 70:30 mixtures of DMF and DMA. Absorption spectra were recorded on a Varian Model 2200 spectrophotometer controlled by an IBM S9001 computer using the computer program CARYSCAN.[20] Low-temperature absorption spectra were measured on samples placed inside an Oxford Instruments CF-204 cryostat cooled by He exchange gas. MCD spectra were recorded at room temperature using a Jasco J500C spectropolarimeter controlled by an IBM S9001 computer using the computer program CDSCAN5,[21] with a field of 5.5 T provided by an Oxford Instruments SM2 superconducting magnet. The MCD signal intensity was calibrated using aqueous cobalt(II) sulfate ($\Delta\epsilon_M(510\text{ nm}) = -1.9 \times 10^{-2}\text{ L mol}^{-1}\text{ cm}^{-1}\text{ T}^{-1}$). Low-temperature MCD spectra were measured on samples placed inside an Oxford Instruments SM4 superconducting magnet.

Data Analysis. As with our previous work,[2a,12-14,22,23] Gaussian band shapes were used to fit the absorption and MCD spectra. Fitting was performed using the program SIMPFIT,[24] which utilizes a Simplex routine, to fit the MCD spectra, and a least-squares minimization routine based on second derivatives, to fit the absorption data. The database management program Spectra Manager[25] was used to manipulate the spectral data.

Results

I. Absorption and MCD Spectra. The number and energies of bands observed between 250 and 800 nm in the absorption and MCD spectra of $(L)_2Fe^{II}Pc$ are highly dependent on the nature of the axially coordinated ligand.[26,27] (The spectral features of iron phthalocyanines also depend on the spin and oxidation state of the coordinated iron.[2a,26-28]). Coordination with strong bases provides a stable complex from which to explore ligation effects on the optical spectra of $Fe^{II}Pc$. Of a number of available bases, ammonia offers the best spectroscopic properties: it binds tightly to $Fe^{II}Pc$ and does not contribute to the absorption spectrum above 250 nm. The spectrum of $(NH_3)_2Fe^{II}Pc(-2)$ is characterized by a resolved B band at 332 nm, a weak band at 425 nm, and an intense Q band at 661 nm (dashed lines in Figure 1A). This spectrum represents the typical low spin $(L)_2Fe^{II}Pc(-2)$ complex in which a charge transfer band is located near 420 nm.[2a,26a,27] Significant changes in the absorption spectral envelope occur when carbon monoxide (CO) is bubbled into a solution of $(NH_3)_2Fe^{II}Pc(-2)$, Figure 1A,B. The major spectral changes observed (Figure 1B) are as follows: a slight blue shift (661 $\rightarrow$ 659 nm) and increased intensity of the Q band; disappearance of the 425-nm band to give a spectral window between 400 and 500 nm; a blue shift of the bands between 250 and 450 nm. The presence of sharp isobestic points near 485, 385, 370, and 335 nm (Figure 1B) indicate the formation of a single new $L_1L_2Fe^{II}Pc(-2)$ complex. Because CO is known to bind *trans* to a basic (σ donor) ligand,[29-32] the complex formed by bubbling CO into a solution of $(NH_3)_2Fe^{II}Pc(-2)$ can be written as $(NH_3)(CO)Fe^{II}Pc(-2)$; the absorption spectrum is shown as the full line in Figure 1A. Absorption maxima measured from the room temperature spectra of a variety of $L_2Fe^{II}Pc(-2)$ complexes are listed in Table 1.

The room-temperature (298 K) MCD spectrum of $(NH_3)(CO)Fe^{II}Pc(-2)$ (Figure 2, bottom spectrum) is characteristic of CO coordination, in which a strong negatively-signed MCD signal, which is associated with a weak absorption band, is observed as the lowest energy transition of the B-band region (at 363 nm). Similar room-temperature features are observed for $(CO)RuPc$[15b].

(16) Sharonov, Y. A. In *Soviet Scientific Reviews, Section D: Physicochemical Biology Reviews*; Skulachev, V. P., Ed., Harwood Academic Publishers: Chur, Switzerland, 1991; Vol. 10(3).
(17) Dawson, J. H.; Dooley, D. M. In *Iron Porphyrins, Part 3*; Lever, A. B. P., Gray, Eds., VCH Publishers: New York, 1988.
(18) Lever, A. B. P.; Pickens, S. R.; Minor, P. C.; Licoccia, S.; Ramaswany, B. S.; Magnell, K. *J. Am. Chem. Soc.* **1981**, *103*, 6800–6806.
(19) Martin, K. A. M. M.Sc. Thesis, The University of Western Ontario, London, Ontario, Canada, 1979.
(20) Ough, E. A.; Stillman, M. J. Unpublished results.
(21) (a) Gasyna, Z.; Browett, W. R.; Nyokong, T.; Kitchenham, R.; Stillman, M. J. *Chemom. Intell. Lab. Syst.* **1989**, *5*, 233–246. (b) Mack, J.; Stillman, M. J. Unpublished results.
(22) Ough, E. A.; Gasyna, Z.; Stillman, M. J. *Inorg. Chem.* **1991**, *30*, 2301–2310.
(23) Ough, E. A.; Creber, K. A. M.; Stillman, M. J. *Can. J. Chem.* **1993**, *71*, 1898–1909.
(24) Browett, W. R.; Stillman, M. J. *Comput. Chem.* **1987**, *11*, 241–250.
(25) Browett, W. R.; Stillman, M. J. *Comput. Chem.* **1987**, *11*, 73–82.
(26) (a) Stillman, M. J.; Thomson, A. J. *J. Chem. Soc., Faraday Trans. 2* **1974**, *70*, 790–804. (b) Stillman, M. J.; Thomson, A. J. *J. Chem. Soc., Faraday Trans. 2* **1974**, *70*, 805–814.
(27) Dale, B. W. *J. Chem. Soc., Faraday Trans.* **1969**, *65*, 331.
(28) (a) Kobayashi, N.; Koshiyama, M.; Ishikawa, Y.; Aso, T.; Shirai, H.; Hojo, N. *Chem. Lett.* **1984**, 1633–1666. (b) Kobayashi, N.; Shirai, H.; Hojo, N. *J. Chem. Soc., Dalton Trans.* **1984**, 2107–2110.
(29) Stynes, D. V.; James, B. R. *J. Am. Chem. Soc.* **1974**, *96*, 2733–2738.
(30) (a) Calderazzo, F.; Papmaloni, G.; Vitali, D.; Pelizzi, G.; Collamati, I.; Frediani, S.; Serra, A. M. *J. Organomet. Chem.* **1980**, *191*, 217–242. (b) Calderazzo, F.; Frediani, S.; James, B. R.; Pampaloni, G.; Reimer, K. J.; Sams, J. R.; Serra, A. M.; Vitalli, D. *Inorg. Chem.* **1982**, *21*, 2302–2306.
(31) James, B. R.; Reimer, K. J.; Wong, T. C. T. *J. Am. Chem. Soc.* **1977**, *99*, 4815.
(32) Calderazzo, F.; Vitalli, D.; Pampaloni, G.; Collamati, I. *J. Chem. Soc., Chem. Commun.* **1979**, 221.

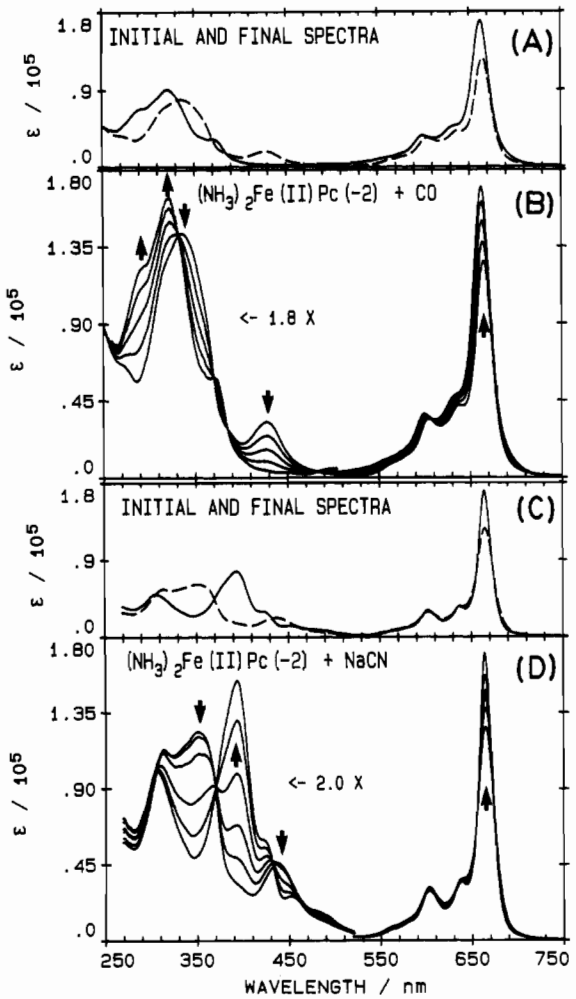

Figure 1. (A) The initial (- - -) and final (—) spectra recorded as CO was bubbled into a solution of $(NH_3)_2Fe^{II}Pc(-2)$. (B) Absorption changes observed during the reaction of CO with $(NH_3)_2Fe^{II}Pc(-2)$ in DCM (the arrows represent the spectral changes as CO was bubbled through the solution). (C) Initial (- - -) and final (—) spectra recorded during the titration of NaCN into a solution of $(NH_3)_2Fe(II)Pc(-2)$. (D) Absorption changes observed during the titration of sodium cyanide (NaCN) into a DMF solution of $(NH_3)_2Fe^{II}Pc(-2)$ (the arrows represent the spectral changes as NaCN was titrated into the solution).

Table 1. Observed Maxima in the Absorption Spectra of the $L_2Fe^{II}Pc(-2)$ species in Dichloromethane

$L_2Fe^{II}Pc(-2)$	λ_{max}/nm				
$Na_2[(CN)_2Fe^{II}Pc(-2)]$	664	602	426	394	310
$(py)_2Fe^{II}Pc(-2)$	651	591	412	328	
$(mepy)_2Fe^{II}Pc(-2)$	652	592	413	331	
$(im)_2Fe^{II}Pc(-2)$	657	596	423	339	
$(meim)_2Fe^{II}Pc(-2)$	658	597	423	338	
$(pip)_2Fe^{II}Pc(-2)$	659	598	425	340	
$(NH_3)_2Fe^{II}Pc(-2)$	661	601	425	332	
$(NH_3)(CO)Fe^{II}PC(-2)$	659	596	363	317	288

At 50 K (Figure 2, top spectrum) the Q band is observed as an extremely sharp band at 659 nm, followed to higher energies by a progression of weak bands assigned as transitions into excited vibronic states.[2a] Significantly, the MCD spectrum exhibits both positive and negative intensity in the vibronic region, unlike the MCD spectra measured previously for other phthalocyanines generally at room temperature. Both absorption and MCD spectra are essentially temperature independent. The additional resolution observed below 77 K allows the individual transitions to be seen more clearly. In particular, it is apparent that the band at 363 nm lacks the derivative-shaped band that is present near 430 nm in $L_2Fe^{II}Pc(-2)$ (L = im, meim, pip, py, mepy, NH_3). The spectral window (400–500 nm) common to MgPc-

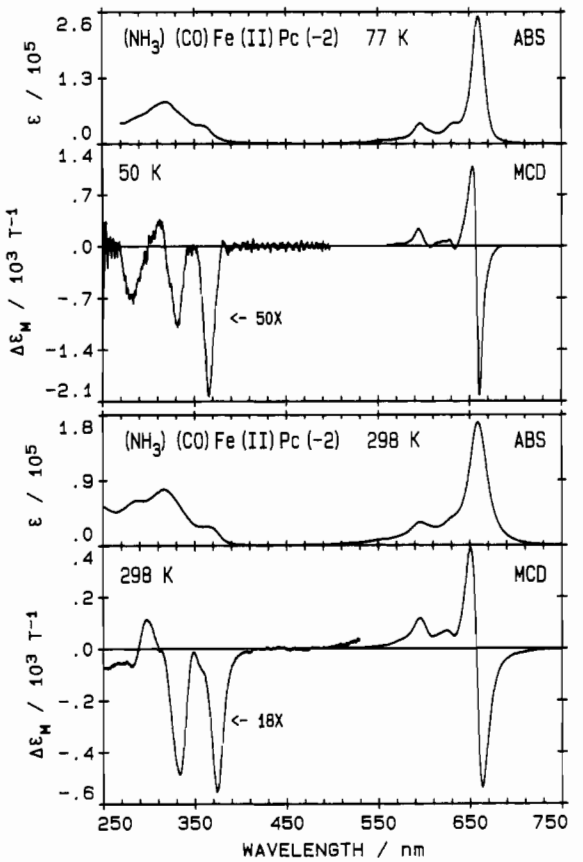

Figure 2. Low-temperature absorption (77 K) and MCD (50 K) spectra (top), and room-temperature (298 K) absorption (ABS) and MCD spectra (bottom) for $(NH_3)(CO)Fe^{II}Pc(-2)$. The room-temperature spectra are recorded in DCM while the low-temperature spectra are recorded in a 70:30 DMF–DMA glass.

(-2)[2a,12] and $ZnPc(-2)$[2a,13–15a] reappears in the $(NH_3)(CO)Fe^{II}$-Pc(–2) spectra.

Titration of sodium cyanide (NaCN) into a solution of $(NH_3)_2$-$Fe^{II}Pc(-2)$ causes significant changes in the absorption and MCD spectra. The changes in the absorption spectrum accompanying addition of cyanide are shown in Figure 1C,D. Unlike the addition of CO (Figure 1B), there are two distinct phases in the titration of NaCN into solutions of $(NH_3)_2Fe^{II}Pc(-2)$. An initial increase in Q-band intensity and a slight blue shift in the 425-nm CT band before the onset of isosbestic changes indicate that formation of $Na[(NH_3)(CN)Fe^{II}Pc(-2)]$ probably occurs as a first product. Sharp isobestic points at 430 and 370 nm are then observed during the conversion of $Na[(NH_3)(CN)Fe^{II}Pc(-2)]$ to $Na_2[(CN)_2Fe^{II}$-Pc(–2)]. The spectral changes observed during the formation of $Na_2[(CN)_2Fe^{II}Pc(-2)]$ include an increase in the Q-band spectral intensity and a red shift (661 → 664 nm) in its energy. The splitting of the two bands that are major contributors to the spectral intensity between 300 and 350 nm in $(NH_3)_2Fe^{II}Pc(-2)$ is a common feature of cyanide complexation,[2a,14,26a] and the room-temperature absorption and MCD spectra of $Na_2[(CN)_2Fe^{II}$-Pc(–2)] (Figure 3) are generally similar to the analogous spectra of $Na[(CN)ZnPc(-2)]$[2a,14,26a] and $Na[(CN)_2Co^{III}Pc(-2)]$.[1,26a]

The room temperature absorption and MCD spectra of $(NH_3)_2$-$Fe^{II}Pc(-2)$ (Figure 4) are distinct from those for main group metallophthalocyanines[2a,12,14,15,19] in that spectral intensity is observed in the 400–550-nm region, which is a spectral window in the "simple" phthalocyanines.[2a,12,14,15,19] Charge transfer transitions are known to contribute to the 400–550 nm spectral intensity in transition metal phthalocyanines.[2a] The derivative shape in the MCD spectra indicates that at least one degenerate transition arises in this region. The CT transitions can extend

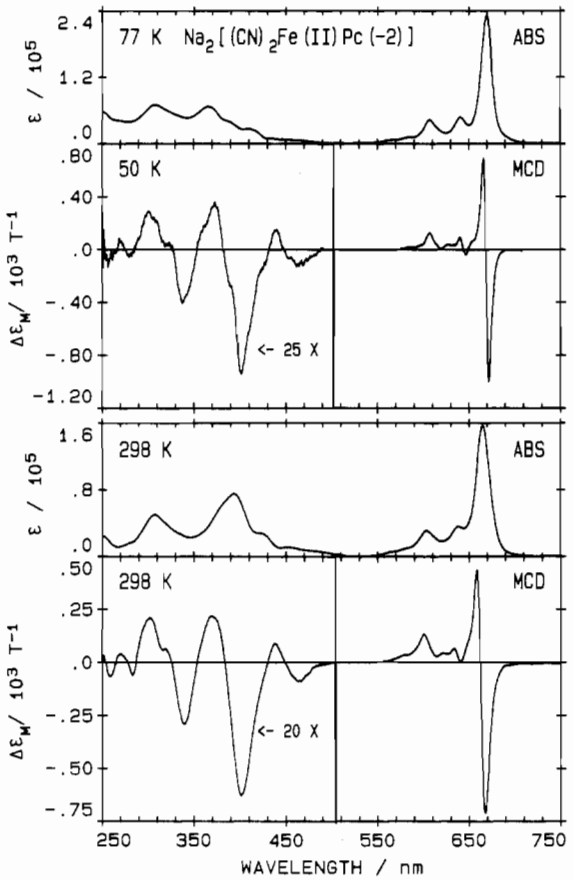

Figure 3. Low-temperature absorption (77 K) and MCD (50 K) spectra (top), and room temperature (298 K) absorption (ABS) and MCD spectra (bottom) for $Na_2[(CN)_2Fe^{II}Pc(-2)]$. The room-temperature spectra are recorded in 98:2 DCM–DMF while the low-temperature spectra are recorded in a 70:30 DMF–DMA glass.

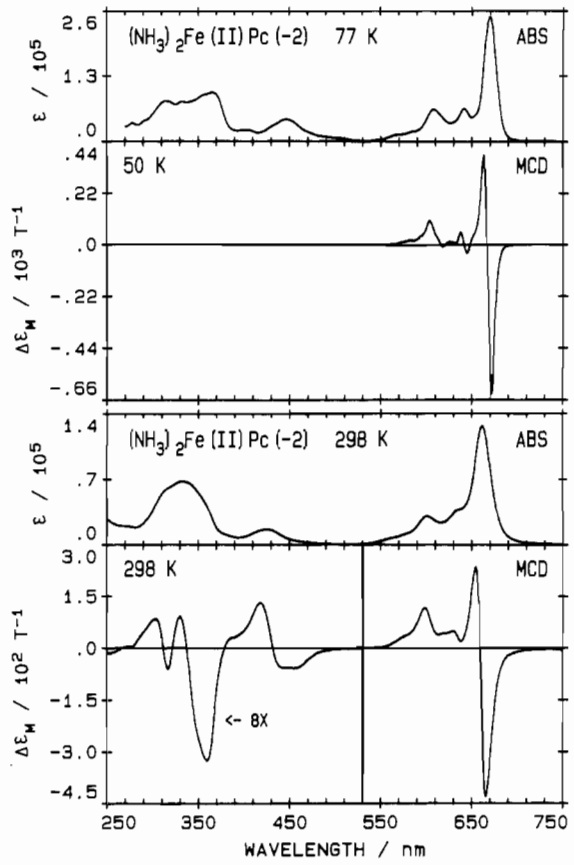

Figure 4. Low-temperature absorption (77 K) and MCD (50 K) spectra (top), and room-temperature (298 K) absorption (ABS) and MCD spectra (bottom) for $(NH_3)_2Fe(II)Pc(-2)$]. The room-temperature spectra are recorded in DCM while the low-temperature spectra are recorded in a 70:30 DMF–DMA glass. Note the changes in the ordinate scale for the MCD traces.

into the B region (250–400 nm), which further complicates the assignment of the ring transitions that occur in this region of the spectrum.[2a]

Low-temperature absorption (77 K) and MCD (50 K) spectra for $(NH_3)_2Fe^{II}Pc(-2)$, $(NH_3)(CO)Fe^{II}Pc(-2)$, and $Na_2[(CN)_2Fe^{II}Pc(-2)]$ are also shown in Figures 2–4. No significant temperature dependence was observed (even to 4 K; data not shown) for these complexes other than an expected sharpening in most bands. This result is important because it allows us to use the room-temperature spectral data, which generally exhibit greater signal to noise ratios, for analysis. The lack of temperature dependence means that the derivative features observed throughout these spectral envelopes can be associated with MCD A terms arising from transitions from a nondegenerate ground state to degenerate excited states. We were unable to obtain reasonable MCD spectra at 50 K for the B region MCD spectrum of $(NH_3)_2Fe^{II}Pc(-2)$ due to the weakness of the MCD signal and the limited solubility of this complex in the solutions used to prepare the glass.

Inspection of the three sets of room- and low-temperature spectra shown in Figures 2–4 indicates that the major changes in the spectra can be associated with band narrowing arising from the formation of the dilute frozen glassy solution. Although no new spectral components become visible at 50 K, the effect of band narrowing in spectral envelopes as complicated as those found for the phthalocyanines allows us to confirm that the parameters used in the deconvolution calculations on room-temperature spectral data are essentially correct. The increase in spectral intensity and the band narrowing at lower temperatures for the entire Q and (Q_{00} and Q_{vib}) is consistent with a depopulation of thermally excited vibronic levels. The red shift in the Q band is attributed to the different solvent systems employed in the room-temperature solutions (DCM) and low-temperature glasses (70:30 DMF:DMA). The sharp and intense A term under the Q band, which is observed at 50 K, does not exhibit features that would indicate the presence of zero-field splitting in the degenerate E_u excited state. Because the Q band is so sharp, zero-field splitting on the order of 20–100 cm^{-1} would be observable from distortion of the derivative A term band shape. The 50 K MCD spectra for the Q region of the three complexes exhibit an unexpected feature. The negatively-signed signal to the blue of the A term is commonly observed for MPc(–2) species, in these spectra we can see that the vibronic component near 640 nm exhibits a negative MCD sign. It appears that this vibronic state may be characterized by an A term centered on an absorption band, which would suggest that this signal arises from a degenerate Q_{vib} state.

It was expected that bands present in the B region would become better resolved in the low-temperature spectra and that the low-temperature spectra could then be employed in spectral deconvolution calculations to enhance the quality of the B region fits. The spectral envelopes in the B region of the low temperature absorption and MCD spectra of $(NH_3)(CO)Fe^{II}Pc(-2)$ (Figure 2) and $Na_2[(CN)_2Fe^{II}Pc(-2)]$ (Figure 3) do not show significant sharpening. This and the poorer quality of the low-temperature B region spectra, compared to the room-temperature spectra, suggests that there is no advantage gained by fitting the low-temperature spectra instead of the room-temperature spectra when both are available.

II. Spectral Band Deconvolution Calculations. Deconvolution results for the Q region (500–750 nm) of these complexes are illustrated by the analysis of the spectral data of $Na_2[(CN)_2Fe^{II}Pc(-2)]$ shown in Figure 5. Seven absorption bands were required to fill the spectral envelope in the Q region. As is the

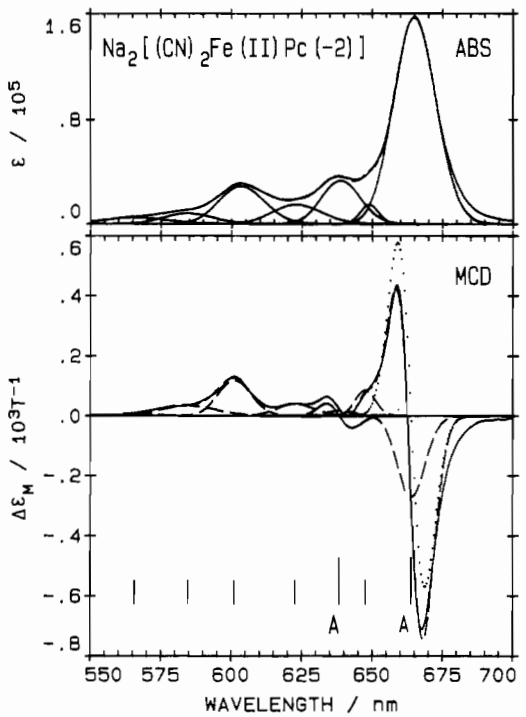

Figure 5. Results of a band analysis of the absorption and MCD spectra for $Na_2[(CN)_2Fe^{II}Pc(-2)]$ in 98:2 DCM–DMF in the visible region (bands 13–30): (a) absorption (—) experimental data, (- - -) fitted data, and (—) individual bands; (b) MCD (—) experimental data, (- - -) fitted data, (···) *A* terms, and (- - -) *B* terms. The band centers of the *A* terms are labeled "A".

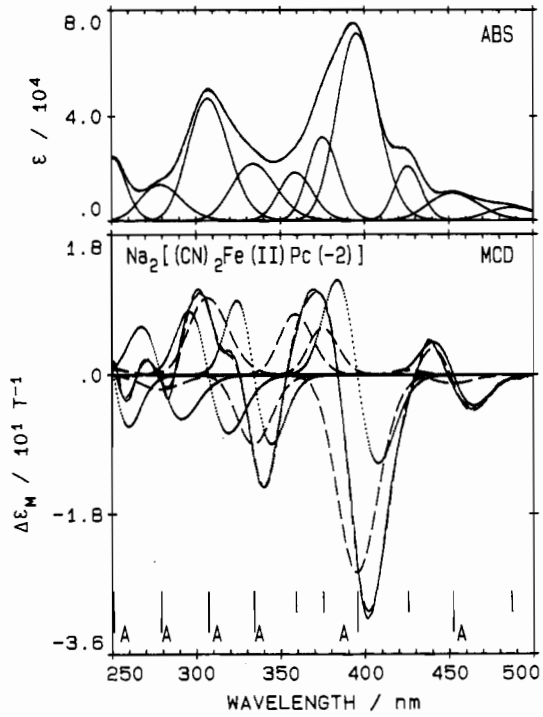

Figure 6. Results of a band analysis of the absorption and MCD spectra for $Na_2[(CN)_2Fe^{II}Pc(-2)]$ in 98:2 DCM–DMF in the ultraviolet region (bands 13–30): (a) absorption (—) experimental data, (- - -) fitted data, and (—) individual bands: (b) MCD (—) experimental data, (- - -) fitted data , (···) *A* terms, and (- - -) *B* terms. The band centers of *A* terms are labeled "A".

case in the Q-band regions of other MPc complexes, we observe the greatest mismatch in fitting to low energy of the Q-band maximum. There is no reason to add extra bands in the MCD fit. Analysis of low-temperature MCD spectra from glassy solutions of ZnPc and $[ZnPc(-3)]^-$ [33] suggests that at room temperature the solvent environment may result in equilibrium between several species, thus broadening the Q band. All but two bands in the Q region were fit to B terms in the MCD spectrum. The absorption bands at 665 nm (15 036 cm^{-1}) and 639 nm (15 654 cm^{-1}) were fit to linked A and B terms in the MCD spectrum. Assignment of the 665-nm transition as the Q_{00} band is consistent with published assignments for $(L)_2MgPc(-2)$ [12] and $(L)ZnPc(-2)$.[13,14] The presence of a second MCD A term in the Q region of MgPc(–2) and ZnPc(–2) has not been rigorously pursued, the recent low-temperature MCD spectra of ZnPc(–2)[33a] similarly suggest the presence of more complicated vibronic interactions than previously described. This transition is assigned as a vibrational component of the Q band (Q_{0x}). While much more intense, negative A terms are associated with the Q_{01} band in metalloporphyrins,[16,17] the vibronic structure of the Q-band region in phthalocyanines is quite different when compared with those of analogous porphyrins.

The absorption and MCD spectra in the B region (230–500 nm) of $(L)_2Fe^{II}Pc(-2)$, L = CO, CN^-, NH_3, are more complicated than the B region spectra of $L_2MgPc(-2)$ [12] and $LZnPc(-2)$,[13,14] An increase in the number of transitions occupying the same spectral range makes it progressively more difficult to obtain a unique fit. The B region fits for ring oxidized MgPc(–1)[22] and ZnPc(–1)[13,14] indicate that the SIMPFIT program[24] yields unique results when a large number of relatively equal intensity bands occupy a narrow spectral region. The B region fits the $Na_2[(CN)_2Fe^{II}Pc(-2)]$ (Figure 6), $(NH_3)(CO)Fe^{II}Pc(-2)$ (Figure 7A) and $(NH_3)_2Fe^{II}Pc(-2)$ (Figure 7B) required 10, 9, and 9 bands, respectively. The parameters used to fit the Q and B regions for the three $L_2Fe^{II}Pc(-2)$ complexes are listed in Tables 2–4. The B region MCD spectra of $(NH_3)_2Fe^{II}Pc(-2)$ (Figure 7B) and $Na_2[(CN)_2Fe^{II}Pc(-2)$ (Figure 6) were fit with six sets of linked *A* and *B* terms, while the additional bands were fit to MCD *B* terms. Five of the nine B region absorption bands in $(NH_3)(CO)Fe^{II}Pc(-2)$ (Figure 7A) were fit to linked MCD *A* and *B* terms. The degenerate band centers obtained from spectral deconvolution, for the entire series of $L_2Fe^{II}Pc(-2)$ complexes studied, are listed in Table 5.

III. Moment Analysis of the Q Region. Table 6 lists the results of a moments analysis of the Q region for $L_2Fe^{II}Pc(-2)$. The moments calculation was carried out using the same program as described previously.[14] Since the program can only analyze well-resolved bands, the analysis was limited to the Q band. The moments calculations provide values for the magnetic moment of the entire Q band excited state[34] (the high energy vibrational bands are included in the calculations). The A_1/D_0 parameter factors out any error in the estimation of the concentration for each solution because the same solution is used for both absorption and MCD measurements.[26b] However, we note that because the moments are calculated by numerical integration over the entire spectral envelope, the values calculated do not correspond to the values obtained by fitting in which a single band shape is used.

Discussion

The "simple" phthalocyanines, such as MgPc(–2) and ZnPc(–2), provide unique opportunities to probe the electronic structure of the phthalocyanine macrocycle. Although these phthalocyanines act as model systems of the naturally occurring porphyrins, the lack of chemistry at the metal site limits their usefulness in the development of artificial systems that mimic the natural processes that occur in heme proteins and enzymes. Studies of

(33) (a) Mack, J.; Stillman, M. J. Unpublished results. (b) Mack, J.; Stillman, M. J. *J. Am. Chem. Soc.*, in press.

(34) Stephens, P. J.; Suetaka, W.; Schatz, P. N.; *J. Chem. Phys.* **1966**, *44*, 4595–4602.

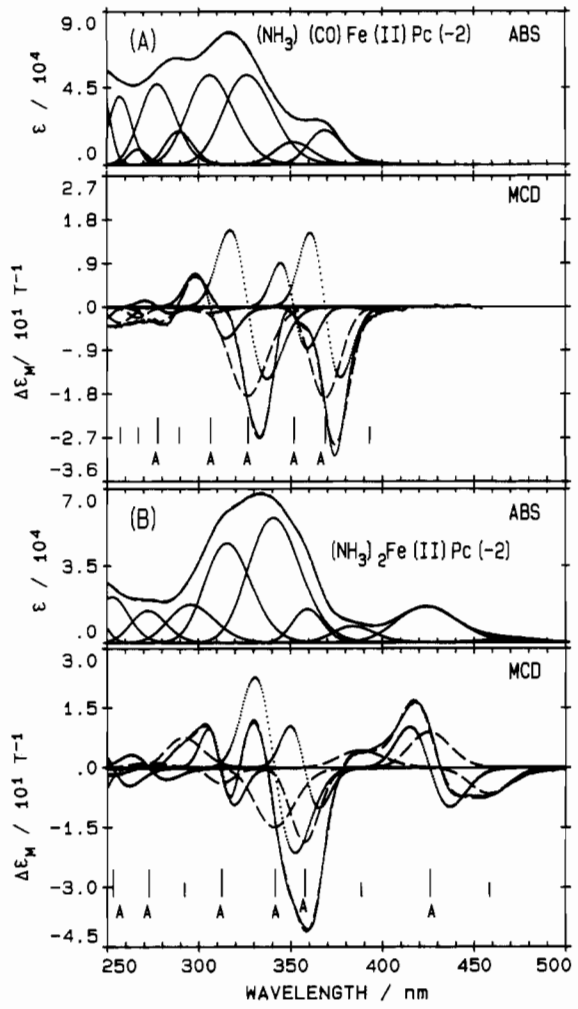

Figure 7. Results of a band analysis in the ultraviolet region of the absorption and MCD spectra for (A) $(NH_3(CO)Fe^{II}Pc(-2)]$ in DCM (bands 14–27) and (B) $(NH_3)_2Fe^{II}Pc(-2)$ in DCM (bands 14–30): (a) absorption (—) experimental data, (- - -) fitted data, and (—) individual bands; (b) MCD (—) experimental data, (- - -) fitted data, (···) *A* terms, and (- - -) *B* terms. The band centers of *A* terms are labeled "A".

iron phthalocyanines show that the central iron atom exhibits a very diverse and interesting chemistry.[2a,26-28,35-40]

Like the iron porphyrins,[16,17] iron phthalocyanine can bind a wide variety of inorganic ligands.[2a,26,27,38] A dissociative mechanism is suggested for the binding of axial ligands in iron porphyrins and iron phthalocyanine.[29] Kinetic studies on CO and RCN binding indicate that the binding constants are 10^3–10^5 times weaker in iron phthalocyanine than in iron porphyrins.[29,38] The discrepancy in K_D values is attributed to the difference in the size of the central hole in the porphyrin and phthalocyanine rings.[29] The smaller hole size in iron phthalocyanine provides greater overlap of the π and π^* orbitals of the phthalocyanine ring with iron 3d orbitals. The greater orbital overlap in iron phthalocyanine results in a larger crystal field splitting. The increased equatorial interaction in iron phthalocyanine results in it being a better π acceptor–σ donor than the iron porphyrins.

Although iron phthalocyanine has been the subject of kinetic studies,[29,37,38,41-43] electrochemical measurements,[42] X-ray crystal structure determinations,[30a,44-46] and Mössbauer,[30b,47-65] ultraviolet–visible,[2a,26-28] and MCD[2a,26,28] spectroscopic studies, there have been few attempts to relate the spectroscopic measurements to the chemical and physical properties of FePc. Spectral deconvolution provides the energies of specific transitions and the effect of axial ligation on these transition energies: parameters that are invaluable to both experimental and theoretical chemists.

The combination of absorption and MCD spectral data allow identification of the major π–π^* bands of the phthalocyanine ring. The data presented here show that at least two other degenerate states exist for $(L)_2Fe^{II}Pc$. These are assigned as metal to ligand charge transfer (MLCT).

I. Band Assignments. $(NH_3)_2Fe^{II}Pc(-2)$. The spectral fits for $(NH_3)_2Fe^{II}Pc(-2)$ required eight degenerate transitions, two more than can be explained by assigning the Q_{00}, Q_{0X}, B1, B2, N, and L transitions. The energy level diagram in Figure 8B outlines specific molecular orbitals and allowed transitions in low spin $Fe^{II}Pc$. Figure 8A illustrates the splitting of the iron(II) 3d orbitals, in $Fe^{II}Pc$, under octahedral ($10Dq$) and tetragonal (Δ_1, Δ_2) ligand fields. The stronger octahedral field, compared to the tetragonal field, is responsible for the $L_2Fe^{II}Pc(-2)$ complexes being low spin ($S = 0$) in solution. The two allowed degenerate MLCT transitions shown in Figure 8B for the low spin ($S = 0$) $^1A_{1g}$ ground state are responsible for the two additional MCD *A* terms. The allowed CT bands, the direction of CT, and the polarization of the transitions are listed in Table 7.

The assignment of the degenerate band at 662 nm (15 114 cm^{-1}) as the Q_{00} band is consistent with the spectral analysis of other $M^{II}Pc(-2)$ complexes.[12-14] The weak MCD A term centered at 639 nm (15 654 cm^{-1}) represents the first assignment of a degenerate Q vibrational band (Q_{0X}). Analysis of the B region is not as simple because of the presence of the overlapping CT bands. To isolate specific transitions within this region, we require

(35) Stillman, M. J. In *Phthalocyanines: Principles and Applications*; Leznoff, C. C., Lever, A. B. P., Eds., VCH Publications: New York, 1993; Vol. 3, Chapter 5, pp 227–296.
(36) Furuya, N.; Yoshiba, H. *J. Electroanal. Chem.* **1989**, *263*, 171–174.
(37) Stynes, D. V. *J. Am. Chem. Soc.* **1974**, *96*, 5942–5943.
(38) Stynes, D. V. *Inorg. Chem.* **1977**, *16*, 1170–1173.
(39) Collamati, I.; Ercolani, C.; Rossi, G. *Inorg. Nucl. Chem. Lett.* **1976**, *12*, 799–802.
(40) Ercolani, C.; Gardini, M.; Monacelli, F.; Pennesim, G.; Rossi, G. *Inorg. Chem.* **1983**, *22*, 2584–2589.
(41) Jones, J. G.; Twigg, M. V. *Inorg. Chem.* **1977**, *16*, 1170–1173.
(42) Jones, J. G.; Twigg, M. V. *Inorg. Chem.* **1969**, *8*, 2120–2123.
(43) Sweigart, D. W. *J. Chem. Soc., Dalton Trans.* **1976**, 1476–1477.
(44) Küppers, H.; Kalz, W.; Homborg, H. *Acta Crys., Sect. C: Cryst. Struct. Commun.* **1985**, *C41*, 1420–1423.
(45) Calderazzo, F.; Pampaloni, G.; Vitali, D.; Collamati, I.; Dessy, G.; Fares, V. *J. Chem. Soc., Dalton Trans.* **1980**, 1965–1968.
(46) Ercolani, C.; Monacelli, F.; Dzugan, S.; Goedken, V. L.; Pennesi, G.; Rossi, G. *J. Chem. Soc., Dalton Trans.* **1991**, 1309–1315.
(47) Ohya, T.; Takeda, J.; Kobayashi, N.; Sato, M. *Inorg. Chem.* **1990**, *29*, 3734–3737.
(48) Kobayashi, N.; Konami, H.; Ohya, T.; Sato, M.; Shirai, H. *Makromol. Chem., Rapid Commun.* **1989**, *10*, 1–4.
(49) Kennedy, B. J.; Murray, K. S.; Homborg, H.; Kalz, W. *Inorg. Chim. Acta* **1987**, *134*, 19–21.
(50) Kennedy, B. J.; Murray, K. S.; Zwack, P. R.; Homborg, H.; Kalz, W. *Inorg. Chem.* **1986**, *25*, 2539–2545.
(51) Dickens, L. L.; Fanning, J. C. *Inorg. Nucl. Chem. Lett.* **1976**, *12*, 1–5.
(52) Kobayashi, N.; Shirai, H.; Hojo, N. *J. Chem. Soc., Dalton Trans.* **1984**, 2107–2110.
(53) Myers, J. F.; Rayner, Canham, G. W.; Lever, A. B. P. *Inorg. Chem.* **1975**, *24*, 461–468.
(54) Ouédraogo, G. V.; More, C.; Richard, Y.; Benlian, D. *Inorg. Chem.* **1981**, *20*, 4387–4393.
(55) Ogoshi, H.; Sugimoto, H.; Watanabe, E.; Yoshida, Z.; Maeda, Y.; Sakai, H. *Bull. Chem. Soc. Jpn.* **1981**, *54*, 3414–3419.
(56) Kennedy, B. J.; Brain, G.; Murray, K. S. *Inorg. Chim. Acta* **1984**, *81*, L29–L31.
(57) Frampton, C. S.; Silver, J. *Inorg. Chim. Acta* **1985**, *96*, 187–191.
(58) Kennedy, B. J.; Murray, K. S.; Zwack, P. R.; Homborg, H.; Kalz, W. *Inorg. Chem.* **1985**, *24*, 3302–3305.
(59) Ohya, J.; Kobayashi, N.; Sato, M. *Inorg. Chem.* **1987**, *26*, 2506–2509.
(60) Ercolani, C.; Paoletti, A. M.; Pennesi, G.; Rossi, G. *J. Chem. Soc., Dalton Trans.* **1991**, 1317–1321.
(61) Dale, B. W. *Mol. Phys.* **1974**, *28*, 503–511.
(62) Grenoble, D. C.; Drickamer, H. G. *J. Chem. Phys.* **1971**, *55*, 1624–1633.
(63) Dale, B. W.; Williams, R. J. P.; Edwards, P. R.; Johnson, C. E. *J. Chem. Phys.* **1968**, *49*, 3445–3449.
(64) Dezsi, I.; Balazs, A.; Molnar, B.; Gorobchenko, V. D.; Lukashevich, I. I. *J. Inorg. Nucl. Chem.* **1969**, *312*, 1661–1666.
(65) Hudson, A.; Whitfield, H. J. *Inorg. Chem.* **1967**, *6*, 1120–1123.

Table 2. Band-Fitting Parameters for $(NH_3)_2Fe^{II}Pc(-2)$ in DCM

band no.	ν/cm^{-1}	λ/nm	$\Delta\nu$/cm^{-1}	D_0[a]	band type	$\langle\Delta\epsilon_M\rangle_n$[b] ($n$ = 0, 1)	A_1, B_0[c]/10^{-3}	$B_0/D_0/10^{-3}$	A_1/D_0	μ[d]
1	15 114	662	325	8.63	A	1645	10800		1.25	2.50
					B	−4.50	−29.5	−3.41		
2	15 522	644	288	0.56	B	0.91	5.99	10.7		
3	15 741	635	305	1.83	A	74.2	487		0.27	0.54
					B	0.52	3.43	1.87		
4	16 102	621	400	1.59	B	1.06	6.93	4.36		
5	16 643	601	477	2.66	B	3.33	21.9	8.23		
6	17 160	583	550	0.92	B	1.11	7.26	7.89		
7	17 782	562	800	0.89	B	0.52	3.40	3.82		
8	21 230	471	1200	0.33	B	−0.38	−2.50	−7.58		
9	23 564	424	1417	3.23	A	642.0	4210		1.30	2.60
					B	0.58	3.82	1.18		
10	26 031	384	1962	1.85	B	0.35	2.32	1.25		
11	27 834	359	1422	2.57	A	554.0	3630.0		1.41	2.82
					B	−1.01	−6.61	−2.57		
12	29 323	341	2154	13.6	A	261.0	17100		1.26	2.52
					B	−1.17	−7.68	−0.56		
13	31 656	316	1670	7.78	A	624.0	4090		0.53	1.06
					B	−0.22	−1.44	−0.19		
14	33 765	296	2701	4.56	B	0.64	4.18	0.92		
15	36 669	273	3008	3.97	A	575.0	3770		0.95	1.90
					B	0.11	0.70	0.18		
16	39 479	253	3197	5.54	A	916.0	6000		1.08	2.16
					B	−0.28	−0.18	−0.03		

[a] $D_0 = \langle\epsilon\rangle_0/326.6$, where the units of D_0 (dipole strength) are D^2 (D = Debye units). [b] $\langle\Delta\epsilon_M\rangle_1$ is the first moment and $\langle\Delta\epsilon_M\rangle_0$ is the zeroth moment of the MCD; when fitting with an A term, the program calculates $\langle\Delta\epsilon_M\rangle_1$ and when fitting with a B term the program calculates $\langle\Delta\epsilon_M\rangle_0$. The Faraday term values, A_1 and B_0, are calculated directly from the moments as follows: $A_1 = \langle\Delta\epsilon_M\rangle_1/152.5$, and $B_0 = \langle\Delta\epsilon_M\rangle_0/152.5$. [c] A_1 data is printed above B_0 data when both A and B terms are used. [d] μ = magnetic moment, calculated as $2(A_1/D_0)$ in units of μ_B (=0.4669 cm^{-1} T^{-1}).

Table 3. Band-Fitting Parameters for $(NH_3)(CO)Fe^{II}Pc(-2)$ in DCM

band no.	ν/cm^{-1}	λ/nm	$\Delta\nu$/cm^{-1}	D_0[a]	band type	$\langle\Delta\epsilon_M\rangle_n$[b], ($n$ = 0, 1)	A_1, B_0[c]/10^{-3}	$B_0/D_0/10^{-3}$	A_1/D_0	μ[d]
1	15 172	659	375	13.6	A	3230	21200		1.56	3.12
					B	−2.94	−19.3	−1.42		
2	15 623	640	200	0.69	B	0.50	3.29	4.77		
3	15 846	631	351	2.24	A	67.7	444.0		0.20	0.40
					B	1.12	7.36	3.29		
4	16 210	617	368	1.37	B	1.17	7.68	5.61		
5	16 745	597	468	2.56	B	3.31	21.7	8.48		
6	17 306	578	518	0.88	B	1.17	7.68	8.73		
7	18 067	554	768	0.84	B	0.48	3.12	3.71		
8	25 387	393	1033	0.16	B	−0.03	−0.17	−1.06		
9	27 110	369	1429	3.45	A	841	5520		1.60	3.20
					B	−1.06	−6.93	−2.01		
10	28 430	352	1374	2.08	A	440.0	2890.0		1.39	2.78
					B	−0.01	−0.04	−0.02		
11	30 588	327	2206	12.3	A	1820	12000		0.98	1.96
					B	−1.42	−9.30	−0.76		
12	32 624	307	2085	10.9	A	668.0	4380.0		0.40	0.80
					B	−0.09	−0.57	−0.05		
13	34 552	289	2097	3.86	B	0.01	0.04	0.01		
14	36 013	278	2108	8.98	A	124	814		0.09	0.18
					B	−0.21	−1.35	−0.15		
15	37 454	267	1669	1.33	B	−0.11	−0.70	−0.53		
16	38 885	257	2210	7.38	B	−0.20	−1.29	−0.17		

[a] $D_0 = \langle\epsilon\rangle_0/326.6$, where the units of D_0 (dipole strength) are D^2 (D = Debye units). [b] $\langle\Delta\epsilon_M\rangle_1$ is the first moment and $\langle\Delta\epsilon_M\rangle_0$ is the zeroth moment of the MCD; when fitting with an A term, the program calculates $\langle\Delta\epsilon_M\rangle_1$ and when fitting with a B term the program calculates $\langle\Delta\epsilon_M\rangle_0$. The Faraday term values, A_1 and B_0, are calculated directly from the moments as follows: $A_1 = \langle\Delta\epsilon_M\rangle_1/152.5$, and $B_0 = \langle\Delta\epsilon_M\rangle_0/152.5$. [c] A_1 data is printed above B_0 data when both A and B terms are used. [d] μ = magnetic moment, calculated as $2(A_1/D_0)$ in units of μ_B (=0.4669 cm^{-1} T^{-1}).

the results obtained from spectral fits of "simple" metallophthalocyanine systems. Low-temperature absorption and MCD spectra of ring-reduced magnesium phthalocyanine ($[MgPc(-3)]^{\bullet-}$)[33b,66] were used to calculate the energy separation between the $e_g(\pi^*) \rightarrow b_{1u}(\pi^*)$ and $e_g(\pi^*) \rightarrow b_{2u}(\pi^*)$ electronic transitions. Because the two degenerate MLCT transitions, namely $e_g(d\pi) \rightarrow b_{1u}(\pi^*)$ (MLCT1) and $e_g(d_\pi) \rightarrow b_{2u}(\pi^*)$ (MLCT2), have the same excited-state molecular orbitals as the two transitions in $[MgPc(-3)^{\bullet-}$, the 2050-cm^{-1} separation of the two transitions in $[MgPc(-3)]^{\bullet-}$ approximates the MLCT1–MLCT2 separation in $L_2Fe^{II}Pc(-2)$. This approach is clearly very approximate because the negative charge on $[MgPc(-3)]^{\bullet-}$ and the 3d electrons of Fe(II) in $L_2Fe^{II}Pc(-2)$ will affect the relative energies of the two sets of transitions and because configuration interaction (CI) with neighboring states can significantly influence the transition energies. However, in a sense we trade these effects for a spectroscopically determined energy from state to state transitions.

The B region (230–500 nm) fit for $(NH_3)_2Fe^{II}Pc(-2)$ (Figure 7B) is an ideal starting point from which to determine the general location of the two MLCT bands in $L_2Fe^{II}Pc(-2)$ complexes. Because CT is generally responsible for the spectral intensity between 400 and 550 nm in transition metal phthalocyanines,[2a,27] the degenerate transition at 424 nm (23 564 cm^{-1}) is assigned as MLCT. The absence of an additional degenerate band between

(66) Mack, J.; Kirby, S.; Ough, E. A.; Stillman, M. J. *Inorg. Chem.* **1992**, *31*, 1717–1719.

Table 4. Band-Fitting Parameters for $Na_2[(CN)_2Fe^{II}Pc(-2)$ in DCM

band no.	ν/cm^{-1}	λ/nm	$\Delta\nu$/cm^{-1}	D_0[a]	band type	$\langle\Delta\epsilon_M\rangle_n$[b] (n = 0, 1)	A_1,B_0[c]/10^{-3}	$B_0/D_0/10^{-3}$	A_1/D_0	μ[d]
1	15036	665	260	8.84	A	1924.0	12600.0		1.43	2.86
					B	−5.00	−32.8	−3.71		
2	15409	649	200	0.63	B	1.18	7.75	12.3		
3	15654	639	257	1.79	A	128.0	838.0		0.47	0.94
					B	0.32	2.10	1.17		
4	16049	623	397	1.20	B	1.06	6.95	5.79		
5	16569	604	381	2.17	B	2.89	19.0	9.05		
6	17106	585	662	1.04	B	1.42	9.32	8.96		
7	17677	566	663	0.61	B	0.23	1.48	2.43		
8	20524	487	1299	1.02	B	0.01	−0.02	−0.02		
9	22091	453	1380	2.15	A	263.0	1720.0		0.80	1.60
					B	−0.08	−0.50	−0.23		
10	23484	426	1009	2.92	B	0.03	0.19	0.07		
11	25274	396	1820	16.7	A	1150.0	7550.0		0.45	0.90
					B	−1.95	−12.8	−0.77		
12	26640	375	1487	5.85	B	0.36	2.33	0.40		
13	27839	359	1797	3.89	B	0.53	3.50	0.90		
14	29914	334	2147	5.10	A	1060.0	6960.0		1.36	2.72
					B	−0.69	−4.50	−0.88		
15	32533	307	2901	13.6	A	1510.0	9920.0		0.73	1.46
					B	0.93	6.15	0.45		
16	35814	279	3585	4.52	A	1590.0	10400.0		2.30	4.60
					B	−0.20	−1.32	−0.29		
17	39829	251	3301	6.49	A	1410.0	9230.0		1.42	2.84
					B	0.68	0.44	0.07		

[a] $D_0 = \langle\epsilon\rangle_0/326.6$, where the units of D_0 (dipole strength) are D^2 (D = Debye units). [b] $\langle\Delta\epsilon_M\rangle_1$ is the first moment and $\langle\Delta\epsilon_M\rangle$ is the zeroth moment of the MCD; when fitting with an *A* term, the program calculates $\langle\Delta\epsilon_M\rangle_1$ and when fitting with a *B* term the program calculates $\langle\Delta\epsilon_M\rangle_0$. The Faraday term values, A_1 and B_0, are calculated directly from the moments as follows: $A_1 = \langle\Delta\epsilon_M\rangle_1/152.5$, and $B_0 = \langle\Delta\epsilon_M\rangle_0/152.5$. [c] A_1 data is printed above B_0 data when both an *A* and *B* terms are used. [d] μ = magnetic moment, calculated as $2(A_1/D_0)$ in units of μ_B (=0.4669 cm^{-1} T^{-1}).

Table 5. Band Centers for the Degenerate Transitions of $L_2Fe^{II}Pc(-2)$ Species Obtained by the Deconvolution of the Absorption and MCD Spectra into MCD *A* Terms

$L_2Fe^{II}Pc(-2)$	band center/nm							
$Na_2[(CN)_2Fe^{II}Pc(-2)]$	665	639	453	396	334	307	279	251
$(py)_2Fe^{II}Pc(-2)$	652	625	411	354	336	311	277	
$(mepY)_2Fe^{II}Pc(-2)$	652	625	411	356	336	311	277	
$(im)_2Fe^{II}Pc(-2)$	658	632	422	361	345	312	270	248
$(meim)_2Fe^{II}Pc(-2)$	659	632	422	361	345	312	271	248
$(pip)_2Fe^{II}Pc(-2)$	659	633	424	358	343	315		
$(NH_3)_2Fe^{II}Pc(-2)$	662	635	424	359	341	316	273	253
$(CO)(NH_3)Fe^{II}PC(-2)$	659	631	369	352	327	307	278	

Table 6. Analysis of the Q-Band Region of the Absorption and MCD Spectra of the $L_2Fe^{II}Pc(-2)$ Complexes by the Method of Moments

L	ν/cm^{-1} [a]	D_0[b]	$\langle\Delta\epsilon_M\rangle_1$[c]	A_1[d]	A_1/D_0	magnetic moment[e]	$\langle\Delta\epsilon_M\rangle_0$[f]	B_0/D_0[g]/10^{-1}
im	15 771	24.8	12 200	80.2	3.23	6.46	3.16	8.36
meim	15 788	27.7	12 600	82.6	2.99	5.98	1.90	4.49
py	15 844	24.6	11 800	77.5	3.15	6.30	1.56	4.16
mepy	15 850	26.1	11 800	77.6	2.98	5.96	2.00	5.03
pip	15 822	19.2	9 160	60.1	3.13	6.26	1.33	4.56
NH_3	15 653	24.9	12 600	82.8	3.32	6.64	1.53	4.02
NH_3/CO	15 709	33.5	17 000	112.0	3.33	6.66	3.25	6.35
CN^-	15 580	25.1	12 500	82.2	3.27	6.54	0.38	0.99

[a] Calculated by setting $\langle\epsilon\rangle_1 = 0$. [b] Calculated from $\langle\epsilon\rangle_0 = 326.6D_0cl$. In this work, concentrations were used in the calculations of ϵ and $\Delta\epsilon$; however, the parameter of interest, A_1/D_0, factors out both *c* and *l*. The units of the dipole strength, D_0 are D^2 (D = Debye units). [c] $\langle\Delta\epsilon_M\rangle_1 = \int\Delta\epsilon(\nu-\nu)\,d\nu$; with units of μ_B, T, and cm^{-1}. [d] $A_1 = \langle\Delta\epsilon_M\rangle_1/326.6\mu_B$ and has units of D^2. [e] Magnetic moment with units of μ_B, calculated from $2(A_1/D_0)$. [f] $\langle\Delta\epsilon_M\rangle_0 = \int\Delta\epsilon\,d\nu$. [g] $B_0/D_0 = \langle\Delta\epsilon_M\rangle_0/(\mu_B\langle\epsilon\rangle_0)$; $\mu_B = 0.4669$ cm^{-1} T^{-1}; B_0 has units of D^2/cm^{-2}.

this band and the Q band (662 nm) verifies its assignment as MLCT1. MLCT2 is more difficult to locate, because it overlaps the B1 and B2 bands in the 280–380-nm region of the spectrum. Spectral deconvolution isolated three degenerate transitions, at 359 nm (27 834 cm^{-1}), 341 nm (29 323 cm^{-1}) and 316 nm (31 656 cm^{-1}). Taking into account the influence of CI, the 4300 cm^{-1} difference between the 359- and 424-nm (MLCT1) bands is comparable to the 2050-cm^{-1} separation of the $e_g(\pi^*) \rightarrow b_{1u}(\pi^*)$ and $e_g(\pi^*) \rightarrow b_{2u}(\pi^*)$ transitions in $[MgPc(-3)]^{\bullet-}$.

Because there is no quantitative measure of the $1b_{1u}(\pi^*)$ and $1b_{2u}(\pi^*)$ orbital energies in $(NH_3)_2Fe^{II}Pc(-2)$ and $[MgPc(-3)]^{\bullet-}$, the 341- and 316-nm bands cannot be ruled out as the MLCT2 band. The spectral fits for $L_2MgPc(-2)$[12] and $LZnPc(-2)$[13,14] are invaluable in separating MLCT2 from B1 and B2. The degenerate band center energies in $L_2Fe^{II}Pc(-2)$ (L = NH_3, CO, CN^-), $LZnPc(-2)$ (L = im, CN^-)[13,14] and $(im)_2MgPc(-2)$[12] are shown in Figure 9. A slight blue shift in the Q_{00} and Q_{0x}, B1, B2, N, and L band center energies and a small increase in the B1–B2 band separation are observed as the central metal changes from magnesium to zinc. These differences indicate a small perturbation of the π-system of the Pc(−2) ring by the filled d shell of Zn(II) is responsible for the spectral differences between ZnPc(−2) and MgPc(−2). Extrapolating to $(NH_3)_2Fe^{II}Pc(-2)$ and the partially filled iron(II) 3d shell, we expect the blue shift and the B1–B2 band separation to increase from (im)ZnPc(−2) to $(NH_3)_2Fe^{II}Pc(-2)$. On the basis of this assumption the bands at 341 and 316 nm are assigned B1 and B2, respectively, and the 357-nm band is accepted as MLCT2. The complete assignment places the N and L bands at 273 nm (36 669 cm^{-1}) and 253 (39 479 cm^{-1}).

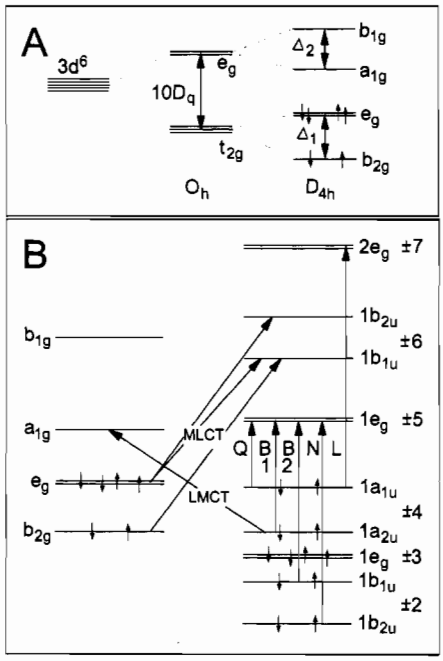

Figure 8. (A) Energy level splitting for the 3d orbitals of the iron(II) ion in a ligand field with cubic ($10Dq$) and axial (Δ_1, Δ_2) distortions. (B) Selected molecular orbitals for the $^1A_{1g}$ ground state of $L_2Fe^{II}Pc(-2)$ showing possible metal-to-ligand charge transfer (MLCT) and ligand-to-metal charge transfer (LMCT) transitions between the low-spin Fe(II) and the phthalocyanine ring.

Table 7. Allowed Charge Transfer Transition for Low-Spin ($S = 0$) Iron(II) Phthalocyanine[a]

one-electron transition	excited state	charge transfer	polarization of transition	MCD term expected
$a_{2u} \rightarrow a_{1g}$	$^1A_{2u}$	L → M	Z	B
$b_{2u} \rightarrow b_{1g}$	$^1A_{2u}$	L → M	Z	B
$b_{2g} \rightarrow b_{1u}$	$^1A_{2u}$	M → L	Z	B
$e_g \rightarrow b_{1u}, b_{2u}$	^1E_u	M → L	XY	A

[a] The ground-state configuration of the iron 3d orbitals is $(b_{2g})^2(e_g)^4$, and the total symmetry of the ground state is $^1A_{1g}$.

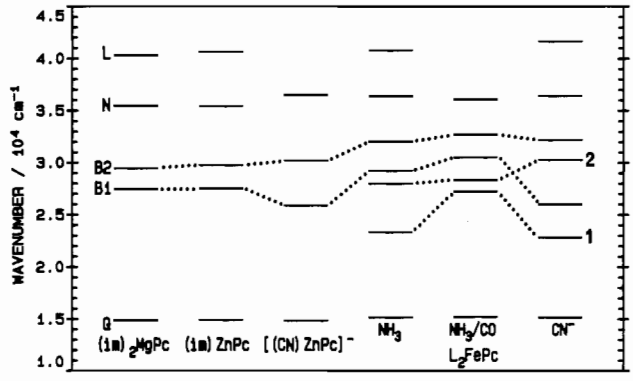

Figure 9. Comparison of the energies of the degenerate bands of $L_2Fe(II)Pc(-2)$ (L = NH_3, CO, CN^-), $LZnPc(-2)$ (L = im, CN^-)[13] and $(im)_2MgPc(-2)$,[12] calculated from deconvolution of the absorption and MCD spectra (band energies summarized in Table 5).

II. Band Assignments. $Na_2[(CN)_2Fe^{II}Pc(-2)]$. Of the eight degenerate transitions required to fit the absorption and MCD spectra of $Na_2[(CN)_2Fe^{II}Pc(-2)]$, the bands at 665 nm (15 036 cm^{-1}), 639 nm (15 654 cm^{-1}), 279 nm (35 814 cm^{-1}), and 251 nm (39 826 cm^{-1}) are assigned to Q_{00}, Q_{0x}, N, and L. The band at 453 nm (22 091 cm^{-1}) is within the CT region and is assigned as MLCT1. Since the B1 and B2 bands are known to split apart in $LZnPc(-2)$,[13,14] the bands at 396 nm (25 274 cm^{-1}) and 307 nm (32 533 cm^{-1}) are assigned to B1 and B2. The final degenerate band at 334 nm (29 914 cm^{-1}) is assigned as MLCT2.

III. Band Assignments. $(NH_3)(CO)Fe^{II}Pc(-2)$. Of the three $L_2Fe^{II}Pc(-2)$ complexes, $(NH_3)(CO)Fe^{II}Pc(-2)$ exhibits the most unique absorption and MCD spectra. Unlike the other two complexes, $(NH_3)(CO)Fe^{II}Pc(-2)$ required seven instead of eight *A* terms to fit the entire MCD spectral envelope (250–800 nm). These data are summarized in Table 3. The Q_{00} and Q_{0X} bands are located at 659 nm (15 172 cm^{-1}) and 631 nm (15 846 cm^{-1}. The presence of five MCD *A* terms in the 250 to 400 nm spectral region indicates a significant blue shift of both ring-bands and MLCT bands. The magnetic moment of 3.20 μ_B from the 369-nm (27 110-cm^{-1}) band compares favorably with the magnetic moment for the MLCT1 band in $(NH_3)_2Fe^{II}Pc(-2)$ (2.60 μ_B) and in $Na_2[(CN)_2Fe^{II}Pc(-2)]$ (1.60 μ_B) and is used to assign this band to MLCT1. The compression of the next three degenerate bands into a narrow spectral region (290–360 nm) makes it difficult to separate MLCT2 from B1 and B2. Since the energy of Q_{00} and Q_{0X} blue shift as a function of ligand ($CN^- < NH_3 < NH_3/CO$) the energies of B1 and B2 are expected to shift to higher energies in $(NH_3)(CO)Fe^{II}Pc(-2)$. The 352-nm (28 321-cm^{-1}) band in $(NH_3)(CO)Fe^{II}Pc(-2)$ is lower in energy than B1 and B2 in $Na_2[(CN)_2Fe^{II}Pc(-2)]$ and is assigned here as MLCT2. The three bands at 327 nm (30 588 cm^{-1})], 307 nm (32 624 cm^{-1}) and 278 nm (36 013 cm^{-1}) are as assigned B1, B2 and N, respectively. The 250-nm spectral cut off in $(NH_3)(CO)Fe^{II}Pc(-2)$ makes it impossible to locate the L band.

IV. Comparison of the Experimental and Predicted Location of MLCT1 in $Na_2[(CN)_2Fe(II)Pc(-2)]$. One of the earliest attempts to assign CT transitions in the electronic spectra of metallophthalocyanines was reported by Lever et al.[18] Lever et al. considered charge transfer to result from either a concerted metal oxidation + ring reduction [i.e. $M^{II}Pc(-2) \rightarrow M^{III}Pc(-3)$; MLCT] or a concerted metal reduction + ring oxidation [i.e. $M^{II}Pc(-2) \rightarrow M^{I}Pc(-1)$; LMCT]. Oxidation and reduction potentials were then used to determine the energies of the two forbidden $e_g(d\pi) \rightarrow 1e_g(\pi^*)$ (MLCT) and $1a_{1u}(\pi) \rightarrow a_{1g}(d)$ (LMCT) and the two allowed $e_g(d\pi) \rightarrow 1b_{1u}(\pi^*)$ (MLCT1) and $1a_{2u}(\pi) \rightarrow a_{1g}(d)$ (LMCT) transitions in a variety of metallophthalocyanines.[18] Because forbidden transitions are considerably weaker and often obscured by allowed transitions and because our primary interest is the assignment of the degenerate transitions, we will focus on MLCT1.

Employing the four relevant electrochemical potentials [+0.93 V for $Fe^{III}Pc(-2)/Fe^{III}Pc(-1)$, +0.14 V for $Fe^{II}Pc(-2)/Fe^{III}Pc(-2)$, −0.99 V for $Fe^{II}Pc(-2)/Fe^{I}Pc(-2)$, and −1.52 V for $Fe^{I}Pc(-2)/Fe^{I}Pc(-3)$] reported for $Na_2[(CN)_2Fe^{II}Pc(-2)]$,[2] we predict the energy of the MLCT1 band to be 24 679 cm^{-1} (405 nm). $Na_2[(CN)_2Fe^{II}Pc(-2)]$ is used here to compare experimental and theoretical results because the electrochemical potentials are not available for either $(NH_3)_2Fe^{II}Pc(-2)$ or $(NH_3)(CO)Fe^{II}Pc(-2)$. Our assignment, based on the deconvolution results for $Na_2[(CN)_2FE^{II}Pc(-2)]$, places MLCT1 at 438 nm, a position which is 2600 cm^{-1} from its predicted location. The discrepancy between theory and experiment is attributed to CI between ground and excited states. Although the energy predicted from the electrochemical assignment was incorrect by several thousand wavenumbers, this is a useful technique to locate the order of CT bands.

V. Effects of Axial Ligation on the Orbital Energies. The band energies obtained by spectral deconvolution for the three $L_2Fe^{II}Pc(-2)$ complexes are plotted in Figure 10. The energies of the degenerate transitions for these three complexes plus five additional $L_2Fe^{II}Pc(-2)$ complexes are listed in Table 5. The band center energies decrease across the ligand series: py > mepy > im > pip > CO/NH_3 > meim > NH_3 > CN^- for the Q_{00} and Q_{0X} bands; CO/NH_3 > mepy > py > im > pip > meim > NH_3 > CN^- for the MLCT1 band; CO/NH_3 > py > mepy > NH_3 > pip > meim > im > CN^- for the B1 band. Comparison of the above series of band center energies with the basicity (σ donor

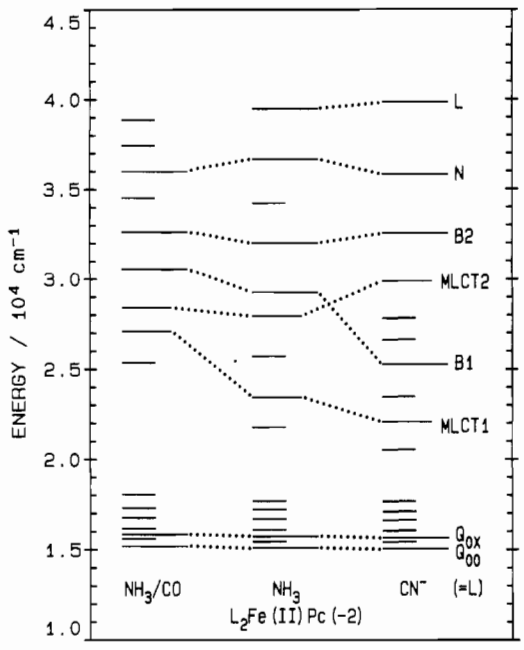

Figure 10. Comparison of the energies of all the bands of $L_2Fe^{II}Pc(-2)$ (L = NH_3, CO, CN^-), calculated from deconvolution of the room-temperature (300 K) absorption and MCD spectra.

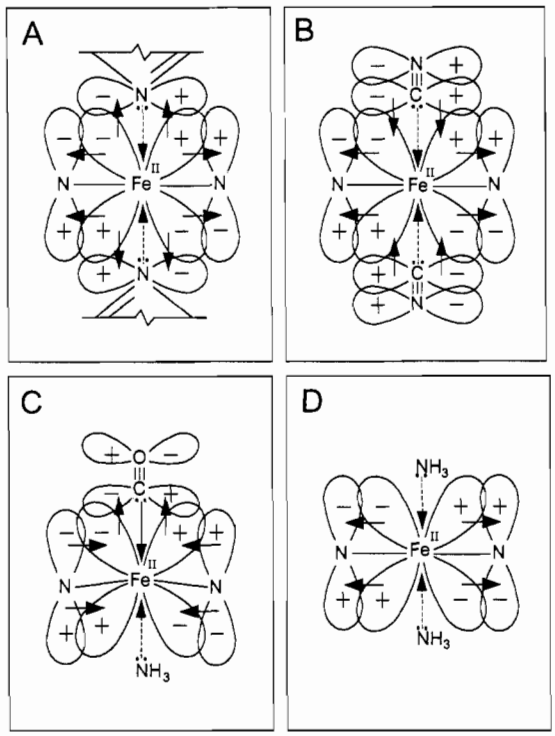

Figure 11. Selected overlapping axial and equatorial π and π^* orbitals in (A) $L_2Fe^{II}Pc(-2)$ (L = im, meim, py, mepy), (B) $Na_2[(CN)_2Fe^{II}Pc(-2)]$, (C) $(NH_3)(CO)Fe^{II}Pc(-2)$, and (D) $(NH_3)_2Fe^{II}Pc(-2)$. The arrows represent the direction of electron donation.

strength) of the axial ligands demonstrates that as the ligand basicity increases across the series[19,54,67,68] there is a red shift in band center energies: CO ≪ py < mepy < im < meim < NH_3 ~ CN^- < pip. Axial σ donation may increase the electron density at the Fe(II) core and reduce equatorial σ donation, thus increasing the electron density at the Pc(-2) ring and decreasing the energy of the state to state transitions.

The overlap of specific orbitals in the axial and equatorial π systems in $L_2Fe^{II}Pc(-2)$ is illustrated in Figure 11. This figure is useful in understanding the minor differences in the ordering of the ligands for the energies of the Q_{00}, Q_{0X}, MLCT1, and B1 bands. Several axial ligands are weak π acceptors and it is clear that back-donation into π^* orbitals affects the separation (cm^{-1}) within the B1–B2 and MLCT1–MLCT2 band pairs. The separation of B1 and B2 increases across the ligand series CO/NH_3 < py < mepy < pip < NH_3 <im ~ meim < CN^-, while the separation of MLCT2 and MLCT1 increases across the ligand series CO/NH_3 < mepy < im < py < mepy < pip < NH_3 < CN^-. The location of CO, the strongest π acceptor ligand, at the beginning of these series suggests that π acceptor strength is inversely proportional to the energy separation. Excluding CN^- and CO, the π acceptor strengths of the axial ligands are small, compared to σ donor strengths, and they are difficult to systematize for the ligand series. In the crystal structure of $(DMSO)_2Fe(II)Pc(-2)$ [45], the S=O bond length (1.474 Å) in the complexed DMSO is not significantly larger than the S=O bond length (1.443 Å) in free DMSO, which indicates only a small π back-bonding effect in the DMSO ligand.

Although the spectral fits of $L_2Fe^{II}Pc(-2)$ [L = py, mepy, im, meim, pip, NH_3] are explained according to the σ donor–π acceptor strengths of the axial ligands, the absorption and MCD results for $Na_2[(CN)_2Fe^{II}Pc(-2)]$ and $(NH_3)(CO)Fe^{II}Pc(-2)$ are difficult to interpret when compared to Mössbauer results.[30,54,55] Quadrupole splittings (ΔE_Q) recorded for intermediate spin iron(II) phthalocyanine complexes were shown to increase across the ligand series: CN^- < CO < CO/NH_3 < im < py < mepy < pip. The value of ΔE_Q is sensitive to the electron density at the Fe(II) core and increases with π acceptor ligands and decreases with σ donor ligands.[19,54,67,68] The small ΔE_Q values for both the CN^- and CO ligands[30,69] are inconsistent with the σ donor–π acceptor strengths of these ligands.

The basicity of CN^- is similar to NH_3, but the B region absorption and MCD spectra of $Na_2[(CN)_2Fe(III)Pc(-2)]$ (Figure 3) are drastically different than those for $(NH_3)_2Fe(II)Pc(-2)$ (Figure 4). The energy level diagram in Figure 10 illustrates the differences in the energies of the degenerate transitions in this region. The smaller ΔE_Q value for the cyanide complex, compared to the complex with NH_3, a weak π acceptor ligand, is inconsistent with the decreased separation of the B1–B2 and MLCT1–MLCT2 band pairs when the axial ligands are switched from CN^- to NH_3. The contradiction between the absorption and the Mössbauer spectra can be addressed by focusing on the π and π^* orbitals in $Na_2[(CN)_2Fe^{II}Pc(-2)]$. Back-donation into the π^* orbitals of CN^- will be inhibited by the negative charge on this ligand. This negative charge favors the removal of electron density from the filled pπ orbitals of CN^-, through the iron dπ orbitals, into the stronger π acceptor Pc(-2) ligand. This coupling of axial and equatorial ligands results in an inductive effect (the arrows in Figure 11 represent this), which increases the π electron density at the Pc(-2) ring, decreases the π electron density at the axial CN^- ligands, and maintains the dπ electron density at the iron core. The infusion of electron density into the π system of the Pc(-2) ring explains the increased separation of the B1–B2 and MLCT1–MLCT2 bands from NH_3 to CN^- while the maintenance of the iron $e_g(d\pi)$ electron density can explain the value of the Mössbauer ΔE_Q parameter.[30,54,65]

The CO ligand in $(NH_3)(CO)Fe^{II}Pc(-2)$ is unique when compared with the other axial ligands since it is both a weak σ donor and a strong π acceptor. Because of this difference in donor–acceptor strengths, it is not unexpected that the absorption and MCD spectra of $(NH_3)(CO)Fe^{II}Pc(-2)$ (Figure 2) are distinct from those for the other $L_2Fe^{II}Pc(-2)$ complexes (Figures 3 and 4). When CO is bound to iron(II) there is an appreciable blue shift in band center energies which are assumed to arise from metal to axial ligand π^* back-donation. The placement of CO

(67) Jones, J. G.; Twigg, M. V. *Inorg. Chim. Acta* **1974**, *10*, 103–104.
(68) Kadish, K. M.; Bottomley, L. A.; Cheng, J. S. *J. Am. Chem. Soc.* **1978**, *100*, 2731–2737.
(69) Dale, B. W.; Williams, R. J. P.; Edwards, P. R.; Johnson, C. E. *Trans. Faraday Soc.* **1968**, *64*, 620.

low in the Mössbauer ligand series imparts serious doubt on this assignment, since the small ΔE_Q values for $L(CO)Fe^{II}Pc(-2)$[30] and $(CO)_2Fe^{II}Pc(-2)$[30b] are unexpected for a weak σ donor and strong π acceptor ligand. The spectral results can be explained by the inductive effect as for the spectral results for cyanide. If the direction of electron flow is reversed for CO ligation, then π electron density is removed from the Pc(-2) ring and introduced into the π^* orbitals of CO with the $e_g(d\pi)$ orbitals of iron as the electron conduit. The loss of π density on the Pc(-2) ring is consistent with the blue shifting of spectral bands and the compression of the B1–B2 and MLCT1–MLCT2 band pairs in the absorption and MCD spectra.

The crystal structure for $(DMF)(CO)Fe^{II}Pc(-2)$[28] provides additional information that can be used to help explain the spectral results. The analysis shows that there is a 0.04-Å displacement of the Fe(II) out of the plane of the Pc ring. This must result in a poorer overlap of the metal and Pc(-2) π orbitals, which may lead to a readjustment of the orbital energies within the molecule.

VI. Moment Analysis. The MCD technique can also provide angular momentum data for excited states as long as the transition is part of an isolated band system.[13,14,26] Stillman and Thomson,[26] Ough et al.,[12] and Nyokong et al.,[13,14] have published Q-band moments for a range of metallophthalocyanines. In $Fe^{II}Pc$, the Q band is completely isolated from CT and other $\pi \rightarrow \pi^*$ transitions. This makes it possible to measure the magnetic moments for a variety of $L_2Fe^{II}Pc(-2)$ complexes. The magnetic moment of the S_1 state (which gives rise to the Q band) for the $L_2Fe^{II}Pc(-2)$ complexes (Table 6) is remarkably constant at 3.0–3.3 (expressed in terms of A_1/D_0). These values are comparable to the A_1/D_0 values of 1.5–3.55 for the $LZnPc(-2)$ complexes[13,14,27] and of 2.43–2.60 for the $L_2MgPc(-2)$ complexes.[12] The greater variation in the A_1/D_0 values for $L_2Fe^{II}Pc(-2)$ and $LZnPc(-2)$, compared to those for $L_2MgPc(-2)$, is interpreted as a difference in response by the three metals to axial ligation, with interaction between metal 3d orbitals and σ and π orbitals of the axial ligands possible for Zn(II) and Fe(II), but impossible for Mg(II).

The difference in the range of magnetic moments for complexes of $L_2Fe^{II}Pc(-2)$ and $LZnPc(-2)$, where the $LZnPc(-2)$ complexes display a greater variability in their A_1/D_0 values, is not understood. The large number of magnetic moments reported here and the influence of axial ligands on the electronic spectra for $L_2Fe^{II}Pc(-2)$ complexes, suggest that $Fe^{II}Pc$ should be an ideal metallophthalocyanine to observe the effects of axial ligation on the magnetic moments. However, from the values reported in Table 6 for the various $L_2Fe^{II}Pc(-2)$ complexes we see that there is no direct correlation between A_1/D_0 values and the donor–acceptor properties of the axial ligands. Although the axial ligands do not appear to influence the magnetic moment of the entire Q band ($Q_{00} + Q_{vib}$), the A_1/D_0 values for isolated Q_{00} bands listed in Tables 2–4 of 1.25 in $(NH_3)_2Fe^{II}Pc(-2)$, 1.56 in $(NH_3)(CO)Fe^{II}Pc(-2)$, and 1.43 in $Na_2[(CN)_2Fe^{II}Pc(-2)]$, which were obtained by deconvolution of the absorption and MCD spectra, indicate a considerable axial ligand effect on the distribution of the total magne tic moment between the Q_{00} and Q_{vib} bands. It appears that in $L_2Fe^{II}Pc(-2)$ complexes with π acceptor ligands (CO), a greater fraction of the magnetic moment is distributed through the Q_{vib} bands, while in π donor ligands a larger portion of the magnetic moment is present in the Q_{00} band.

Conclusions

Three distinct sets of absorption and MCD spectra are observed for low spin $L_2Fe^{II}Pc(-2)$ complexes, according to the donor–acceptor strengths of the axial ligands. These complexes can be separated into groups associated with (i) strong σ donors and weak π acceptors ($L_2Fe(II)Pc(-2)$ (L = im, meim, py, mepy, pip, NH_3)), (ii) strong σ and π donors ($Na_2[(CN)_2Fe^{II}Pc(-2)]$), and (iii) weak σ donor and strong π acceptor (CO in $(NH_3)(CO)Fe^{II}Pc(-2)$), based on the different spectral patterns observed. Deconvolution calculations located transitions to degenerate states at 662 (Q_{00}), 424 (MLCT1), 359 (MLCT2), 341 (B1), 316 (B2), 273 (N), and 253 nm (L) for $(NH_3)_2Fe(II)Pc(-2)$; 665 (Q_{00}), 453 (MLCT1), 396 (B1), 334 (MLCT2), 307 (B2), 279 (N), and 251 nm (L) for $Na_2[(CN)_2Fe^{II}Pc(-2)]$; and 659 ($Q_{00}$), 369 (MLCT1), 352 (MLCT2), 327 (B1), 307 (B2), and 278 nm (L) for $(NH_3)(CO)Fe^{II}Pc(-2)$. Analysis of the spectral fits determined that the axial ligands effect the electronic spectra of $Fe^{II}Pc(-2)$ in three ways: (i) increasing the σ donor strength of the axial ligands decreases the energy of the degenerate transitions; (ii) increasing the π acceptor strength of the axial ligand decreases the separation between the B1–B2 and MLCT1–MLCT2 transitions; (iii) increasing the π donor strength of the axial ligands increases the separation between the B1–B2 and MLCT1–MLCT2 transitions.

Acknowledgment. We thank the NSERC of Canada for financial support. The authors are members of the Centre for Chemical Physics and the Photochemistry Unit at the University of Western Ontario and acknowledge their continuing support of this research. This is Contribution No. 493 from the Photochemistry Unit at the UWO.